NASA Technical Memorandum 2016-219221

December 2016

Passive Rocket Diffuser Testing:

Reacting Flow Performance of Four Second-Throat Geometries

Daniel R. Jones
NASA Stennis Space Center
Stennis Space Center, Mississippi

Daniel C. Allgood
NASA Stennis Space Center
Stennis Space Center, Mississippi

Grady P. Saunders
Jacobs Technology Inc.
Tullahoma, Tennessee

National Aeronautics and
Space Administration

NASA STI Program in Profile

Since its founding, NASA has been dedicated to the advancement of aeronautics and space science. The NASA scientific and technical information (STI) program plays a key part in helping NASA maintain this important role.

The NASA STI program operates under the auspices of the Agency Chief Information Officer. It collects, organizes, provides for archiving, and disseminates NASA's STI. The NASA STI program provides access to the NTRS Registered and its public interface, the NASA Technical Reports Server, thus providing one of the largest collections of aeronautical and space science STI in the world. Results are published in both non-NASA channels and by NASA in the NASA STI Report Series, which includes the following report types:

TECHNICAL PUBLICATION.
Reports of completed research or a major significant phase of research that present the results of NASA Programs and include extensive data or theoretical analysis. Includes compilations of significant scientific and technical data and information deemed to be of continuing reference value. NASA counter-part of peer-reviewed formal professional papers but has less stringent limitations on manuscript length and extent of graphic presentations.

TECHNICAL MEMORANDUM.
Scientific and technical findings that are preliminary or of specialized interest, e.g., quick release reports, working papers, and bibliographies that contain minimal annotation. Does not contain extensive analysis.

CONTRACTOR REPORT. Scientific and technical findings by NASA-sponsored contractors and grantees.

CONFERENCE PUBLICATION.
Collected papers from scientific and technical conferences, symposia, seminars, or other meetings sponsored or co-sponsored by NASA.

SPECIAL PUBLICATION.
Scientific, technical, or historical information from NASA programs, projects, and missions, often concerned with subjects having substantial public interest.

TECHNICAL TRANSLATION.
English-language translations of foreign scientific and technical material pertinent to
NASA's mission.

Specialized services also include organizing and publishing research results, distributing specialized research announcements and feeds, providing information desk and personal search support, and enabling data exchange services.

For more information about the NASA STI program, see the following:

Access the NASA STI program home page at
http://www.sti.nasa.gov

E-mail your question to
help@sti.nasa.gov

Phone the NASA STI Information Desk at
757-864-9658

Write to:
NASA STI Information Desk
Mail Stop 148
NASA Langley Research Center
Hampton, VA 23681-2199

NASA Technical Memorandum 2016-219221

December 2016

Passive Rocket Diffuser Testing:

Reacting Flow Performance of Four Second-Throat Geometries

Daniel R. Jones
NASA Stennis Space Center
Stennis Space Center, Mississippi

Daniel C. Allgood
NASA Stennis Space Center
Stennis Space Center, Mississippi

Grady P. Saunders
Jacobs Technology Inc.
Tullahoma, Tennessee

National Aeronautics and
Space Administration

ACKNOWLEDGEMENTS

The authors would like to thank the entire team of engineers and technicians at SSC who supported this test program. In addition, we would like to acknowledge the leadership of the following individuals:

- Ronnie Rigney – Program Manager
- Gary Taylor – Project Manager
- Andy Guymon – Lead Test Conductor
- Derek Zacher – Systems Engineer
- Harry Ryan – Design and Analysis Lead
- Aaron Head – Controls Engineer
- Astor Pastoral – High Speed Data Engineer
- Peter Tran – Supporting Test Conductor

ABSTRACT

Second-throat diffusers serve to isolate rocket engines from the effects of ambient back pressure. As one of the nation's largest rocket testing facilities, the performance and design limitations of diffusers are of great interest to NASA's Stennis Space Center. This paper describes a series of tests conducted on four diffuser configurations to better understand the effects of inlet geometry and throat area on starting behavior and boundary layer separation. The diffusers were tested for a duration of five seconds with a 1455-pound thrust, LO_2/GH_2 thruster to ensure they each reached aerodynamic steady state. The effects of a water spray ring at the diffuser exits and a water-cooled deflector plate were also evaluated. Static pressure and temperature measurements were taken at multiple axial locations along the diffusers, and Computational Fluid Dynamics (CFD) simulations were used as a tool to aid in the interpretation of data. The hot combustion products were confirmed to enable the diffuser start condition with tighter second throats than predicted by historical cold-flow data or the theoretical normal shock method. Both aerodynamic performance and heat transfer were found to increase with smaller diffuser throats. Spray ring and deflector cooling water had negligible impacts on diffuser boundary layer separation. CFD was found to accurately capture diffuser shock structures and full-flowing diffuser wall pressures, and the qualitative behavior of heat transfer. However, the ability to predict boundary layer separated flows was not consistent.

NOMENCLATURE

A	Area
CFD	Computational Fluid Dynamics
D	Diameter
FSS	Free Shock Separation
gpm	Gallons per Minute
L	Length
$\dot{m}$	Mass Flow Rate
M	Mach Number
O/F	Oxidizer-to-Fuel Ratio
P	Pressure
PL	Power Level
r	Radius
RSS	Restricted Shock Separation
SSC	Stennis Space Center
T	Temperature
TOP	Thrust Optimized Parabolic
t	Time
x	Axial Location
y+	Non-Dimensional Wall Spacing
γ	Ratio of Specific Heats
θ	Angle
$\rightarrow$	Attribute Between Stations

SUBSCRIPTS

a	Ambient Condition
cc	Combustion Chamber
cell	Test Cell
D	Diffuser
DC	Diffuser Contraction
DE	Diffuser Exit
DI	Diffuser Inlet
DfP	Deflector Plate
I	Initial
min	Minimum
NE	Nozzle Exit
NT	Nozzle Throat
ST	Second Throat
Start	Start Condition
0	Stagnation Condition
15°	Property of a 15° Conical Nozzle

INTRODUCTION

NASA's Stennis Space Center (SSC) routinely employs passive second-throat diffusers for altitude testing of liquid rocket engines. Diffuser design has historically been a semi-empirical process incorporating cold-flow data acquired by NASA [1] and the Arnold Engineering Development Complex (AEDC) in the 1960s [2]. Over time, the advancement of Computational Fluid Dynamics (CFD) has facilitated increasingly higher-fidelity analysis of diffuser flow fields and has suggested a significant amount of conservatism in the historical methods when applied to chemically reacting flows [3]. However, no sufficient hot-fire diffuser test data was discovered within the surveyed literature to validate CFD's predictions of diffuser start, boundary layer separation, or heat transfer.

The principal objective of the current work was to develop a reliable method for design and analysis of full-scale rocket diffusers. Therefore, a combined experimental and computational effort was undertaken to determine whether current CFD methodologies being used by SSC were able to accurately capture critical diffuser flow dynamics at a representative subscale in a reacting flow environment. The experimentation presented in this paper was carried out at SSC between May and August 2015.

TEST OBJECTIVES AND CONFIGURATIONS

The primary objective of this test series was to approximate a generic full-scale rocket/diffuser configuration and capture the sensitivities of starting pressure, heat flux, and boundary layer separation to inlet geometry, throat size, downstream cooling water sprays, and deflector location. Testing was conducted at the E-3 test stand. E-3 has frequently been used for testing of both full scale [4] and subscale [5] rocket engines, passive and active diffusers [6], refractory [7] and water-cooled plume deflectors [8], and for simulating water suppression of rocket exhaust acoustics [9].

A liquid oxygen/gaseous hydrogen (LO_2/GH_2) thruster was designed with a maximum chamber pressure of 1148 psia and a nominal oxidizer-to-fuel ratio of 6. The nozzle throat diameter was set at 1.03” to enable a 5-second test duration with an existing LO_2 tank. The expansion ratio was chosen to produce nozzle exit conditions characteristic of the full-scale engines tested at SSC. A thrust-optimized parabolic (TOP) nozzle contour was generated by Rao’s method [10,11] using the parameters listed in Table 1. The combustion chamber and nozzle throat were fabricated from copper and were water cooled during testing. The rest of the nozzle contour was manufactured from a block of stainless steel and was left uncooled. Nominal propellant flow rates and chamber pressures corresponding to several facility-driven power levels are given in Table 2.

D_{NT}	θ_I	θ_{NE}	A_{NE}/A_{NT}	1D M_{NE}	$L/L_{15°}$
1.03″	34°	6°	36.5	4.46	0.85

Table 1 - TOP Nozzle Contour Definition

Power Level	GH_2 (lbm/s)	LO_2 (lbm/s)	P_{CC} (psia)
50%	0.28	1.70	574
81%	0.46	2.75	932
100%	0.57	3.39	1148

Table 2 – Thruster Power Levels and Flow Rates

Four diffuser geometries were generated to provide an array of variables for testing and were constructed of carbon steel. Diffuser #1 was designed using AEDC's semi-empirical methods and was considered a good baseline for comparing hot-fire performance to historical cold-gas data. Diffusers #2 and #3 were generated using CFD to refine the geometry and provide improved performance over Diffuser #1 with the additional goal of independently varying throat area. Diffuser #4 was not conceived until testing of the other three geometries had been completed, and was fabricated by welding the conical inlet of Diffuser #1 to the contraction of Diffuser #3 to lower A_{ST}/A_{DI} below the historically-predicted limit. Graphical depictions of the nozzle/diffuser configurations are given in Fig. 1, and their parametric descriptions are provided in Table 3. For all configurations, the diffuser inlet was in plane with the nozzle exit. The complete test configuration is shown in Fig. 2. Fig. 3 gives a cut-away detail of the thruster, nozzle extension, test cell, and Diffuser #1's inlet. Fig. 4 displays the system during a test of Diffuser #1, as captured by a facility video camera.

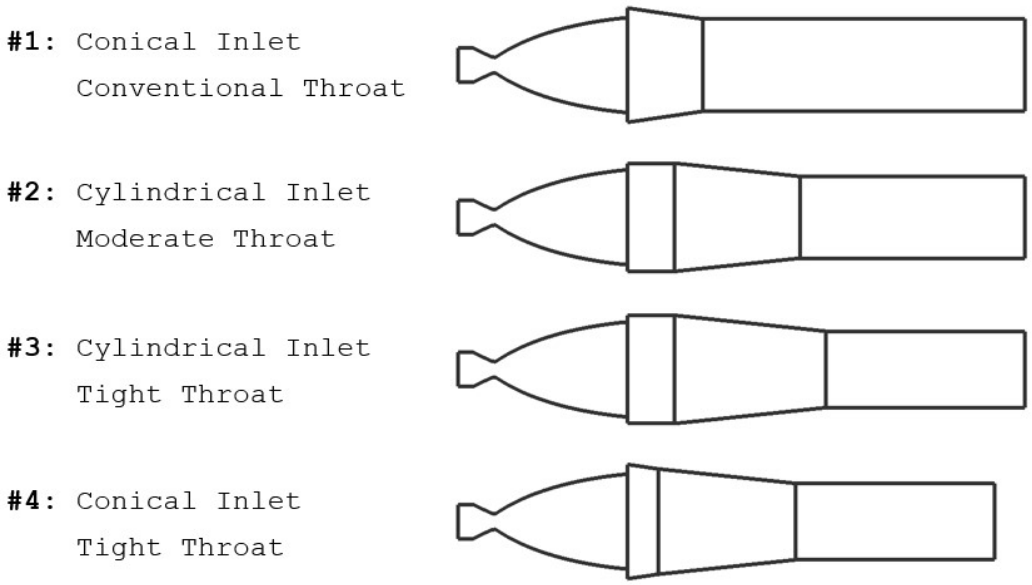

Fig. 1 - Second-Throat Nozzle/Diffuser Configurations

Diffuser	A_{DI}/A_{NE}	A_{ST}/A_{NE}	A_{ST}/A_{DI}	$(L/D)_{DT}$	L_D/D_{DT}	θ_{DC} (°)
#1	1.44	0.94	0.65	3.50	4.32	8.30
#2	1.29	0.74	0.57	2.75	4.87	5.97
#3	1.29	0.65	0.50	2.61	5.21	5.97
#4	1.44	0.65	0.45	2.61	4.82	8.3, 5.97

Table 3 - Diffuser Geometry Parameters

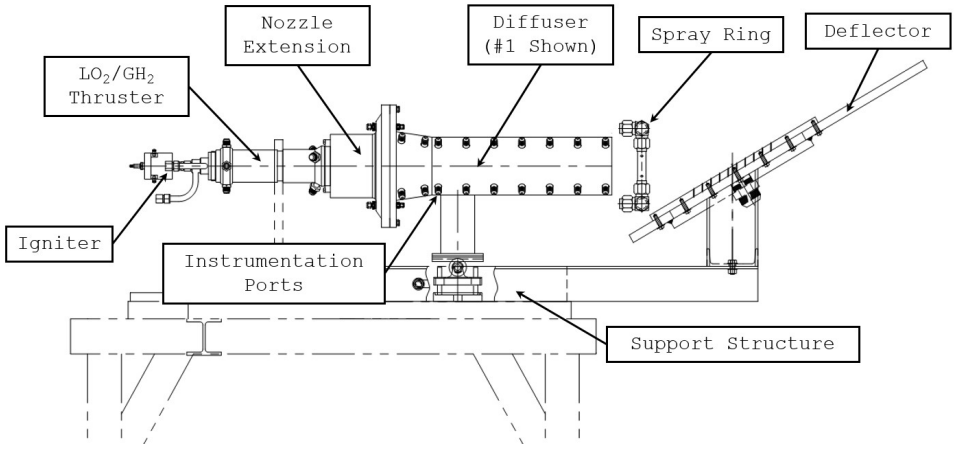

Fig. 2 – System Overview

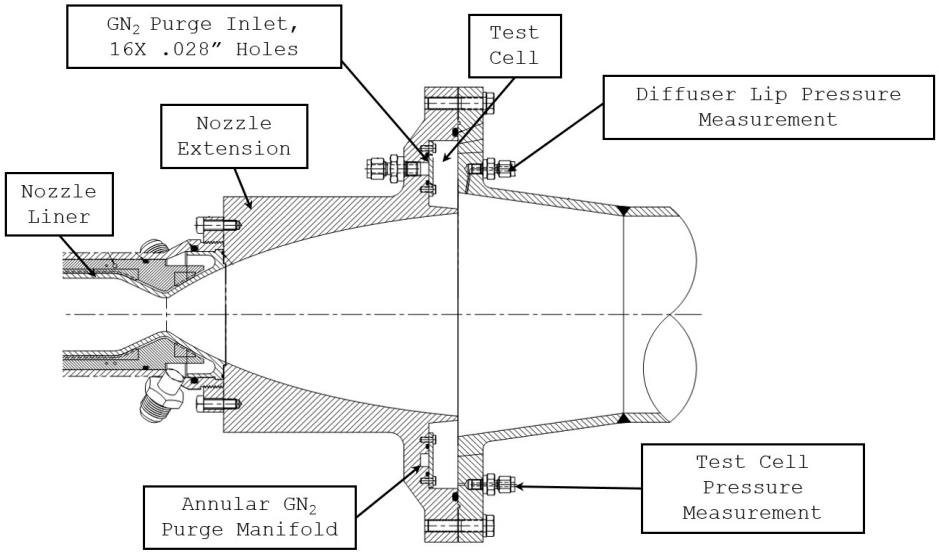

Fig. 3 – Cut-Away Detail of Nozzle, Test Cell, and Diffuser Inlet

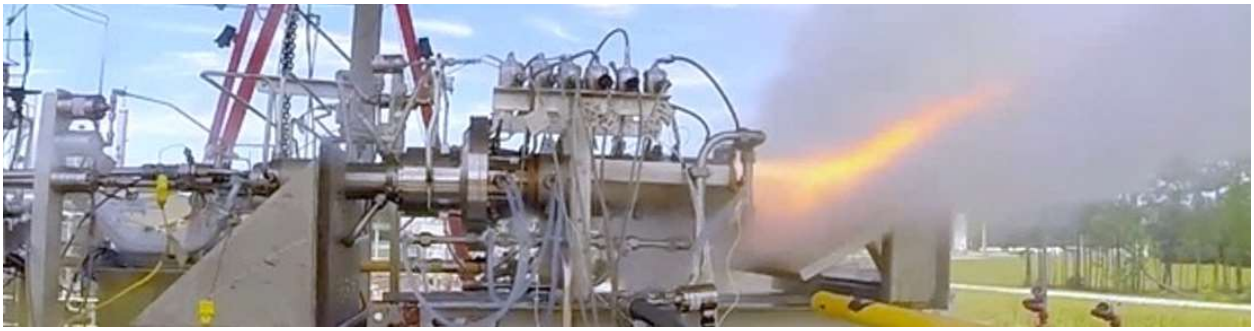

Fig. 4 – Hot-Fire Test of Diffuser #1

Gaseous Nitrogen (GN_2) was employed to inert the test cell at several purge-to-exhaust flow rates which span the range typically used in full-scale engine tests at SSC. The injection occurred through a set of sixteen 0.028" diameter holes evenly distributed circumferentially throughout the upstream wall of the test cell. A list of purge flow rates and pressures are supplied in Table 4. Unless otherwise specified, all tests should be assumed to have been performed at purge level A.

Purge Level	GN_2 Flow (lbm/s | scfm)	P_0 (psig)
A	.00498 | 0.069	100
B	.0125 | 0.172	250
C	.0249 | 0.344	500
D	.0498 | 0.687	1000
E	.0996 | 1.375	2000

Table 4 - GN_2 Purge Flow Rates and Pressures

A spray ring was used to inject water directly into the effluent at the exit of the diffuser to cool the plume before impingement on the deflector plate, as well as suppress the acoustics being generated. The spray ring was essentially a square of tubing with two 25/64" diameter holes on each side that could be rotated to spray into the plume at different angles. The spray ring was fed by a 150 psig water supply. The baseline configuration is shown in Fig. 5. This pattern was later modified so that opposing pairs of holes were slightly offset from one another to avoid splashback into the diffusers. Water was also injected from the deflector plate itself, at a 90° angle to the plume axis. The deflector remained at a fixed location, with its plane at a 30° angle with respect to the plume's axis. However, due to the varying lengths and diameters of the diffusers, the distance from diffuser exit to the deflector plate normalized by the diffuser throat diameter ranged from 2.36 to 3.25. The deflector's water hole pattern is shown in Fig. 6 and was also fed by a 150 psig supply. The water spray ring and deflector plate each produced a cooling water flow rate of 26.4 lbm/s when enabled.

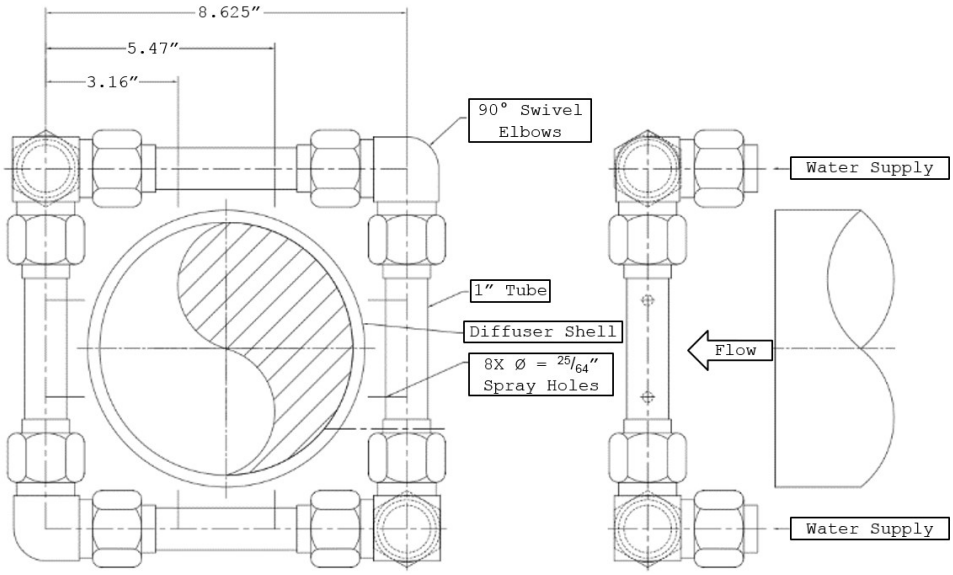

Fig. 5 – Water Spray Ring Configuration

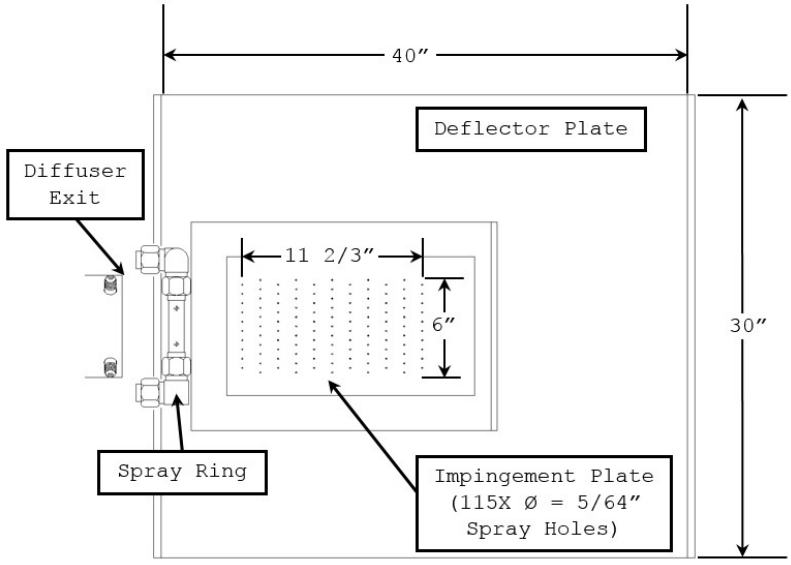

Fig. 6 – Deflector Plate and Water Hole Pattern (Top View)

Table 5 shows a list of key instrumentation. All data presented in this report was sampled at a frequency of 250 Hz.

Location	Measurement	Quantity	Model/Method
GH2 Feed Line	Mass Flow	1	Sonic Choke Orifice (typical diameter=0.286 in)
LO2 Feed Line	Mass Flow	1	Hoffer Turbine Flow Meter (1101X1-4-60) with a Downstream Cavitating Venturi
Spray Ring Inlet	Mass Flow	1	Hoffer Turbine Flow Meter (HO2X2-22-225-CB-1MX-MS-X) with a Downstream Cavitating Venturi
Deflector Inlet	Mass Flow	1	Same as Spray Ring (HO2X2-22-225-CB-1MX-MS-X)
Igniter	Pressure	2	Stellar, 0-2 kpsig
Combustion Chamber	Pressure	2	Stellar, 0-2 kpsig
Test Cell	Pressure	2	Stellar, 0-20 psia
Diffuser Wall	Temperature	11*	Medtherm (TCS-061-K-1.5-10F-36-11038) Type K high response coaxial surface mount thermocouple
Diffuser Wall	Pressure	11*	Stellar, 0-20 psia
GN2 Feed Line	Pressure	1	Stellar, 0-3 kpsig
*Denotes the maximum number of sensors available. Some tests had sensors fail, and others were limited by the physical dimensions.			

Table 5 - Key System Instrumentation

CFD CODE OVERVIEW AND INPUTS

The Loci/CHEM CFD code was employed in the design and analysis of all diffusers found in this report, and its results are shown alongside data in the following sections of this paper. The code is being developed by Mississippi State University with funding from multiple government agencies. Loci is a rule-based program control framework in which an application is described in terms of a collection of simple computational kernels [12]. CHEM is a second-order accurate, density-based flow solver built on the Loci framework. Key features of CHEM include multiple turbulence models, compressibility correction, inviscid flux limitation, finite-rate

chemistry, real-fluid equations of state, Eulerian and Lagrangian multiphase models, support for generalized unstructured meshes, adaptive meshing, and automatic dynamic partitioning. A detailed description of theoretical and numerical formulation may be found in the Loci/CHEM User's manual [13]. CHEM has been used extensively by the CFD team at NASA Stennis and has been found to reliably predict diffuser flows, including boundary layer separation, shock structure, and pressure fields. Table 6 lists Loci/CHEM settings representative of the CFD cases reported in this paper. Inflow temperature and chemical species were obtained using NASA's Chemical Equilibrium with Applications code (CEA).

Spatial Dimensionality:	2D Axisymmetric
Equation of State:	Calorically Imperfect Ideal Gas
Spatial Discretization:	2nd Order
Temporal Discretization:	2nd Order Implicit
Time Step:	1e-4 s (Global)
Iterations:	100,000
Turbulence Model:	Menter's Baseline
Compressibility Correction:	Wilcox
Boundary Layer Model:	Compressible Wall Functions
Chemical Reactions:	Shang's 7s7r H_2/Air Finite Rate Mechanisms [14]
Phase Change:	None
Secondary Flow:	P_0 = 100, 250, 500, 1000, 2000 psia T_0 = 300 K Turbulence Intensity = 10% Mass Fractions: N2 = 1.0
Initial Conditions:	Quiescent Standard Sea Level
Injector Inflow Conditions:	P_{cc} = 1148, 932, or 574 psia T_{cc} = 3544 K Turbulence Intensity = 10% Mass Fractions: H2O = 0.874, OH = 0.068, H2 = 0.038, O2 = 0.011, O = 0.006, H = 0.003

Table 6 – Representative Loci/CHEM Inputs

AERODYNAMIC PERFORMANCE

Start and Shutdown Dynamics

Transient thruster firing characteristics were key to understanding diffuser aerodynamic performance. Fig. 7 shows P_{cc} and O/F vs. time for every test performed during this series. Chamber pressure rose to a steady state faster with a higher commanded P_{cc}, reaching a consistent level in a maximum of ~1.5s in the 50% PL case. Of note is a detonation event that occurred during a commanded 81% PL test in which the igniter malfunctioned and the initiation of combustion was delayed. The delay allowed propellants to fill and subsequently mix inside the combined volume of the engine and diffuser. Once the igniter properly engaged, the conditions in the chamber caused a flame acceleration to occur, and the resultant pressure wave was confirmed to reach the theoretical Chapman-Jouget detonation conditions via high-speed PCB pressure transducers which were mounted along the length of the diffuser. After the explosion event had occurred, the combustion chamber pressure recovered and the diffuser started normally. This off-nominal detonation event has been explained in greater detail in NASA/TP-2016-219220 [15].

Fig. 7 also depicts the consistency in the O/F ramp rate between power levels. However, in comparision to chamber pressure, the mixture ratio suffered greater drift and took almost twice as long (~3s) to reach a steady-state condition. The spike depicted in the O/F data around t=1s was the result of electrical interference and was not noted in the LOX feed system pressure measurement, which was located just upstream of the flow meter.

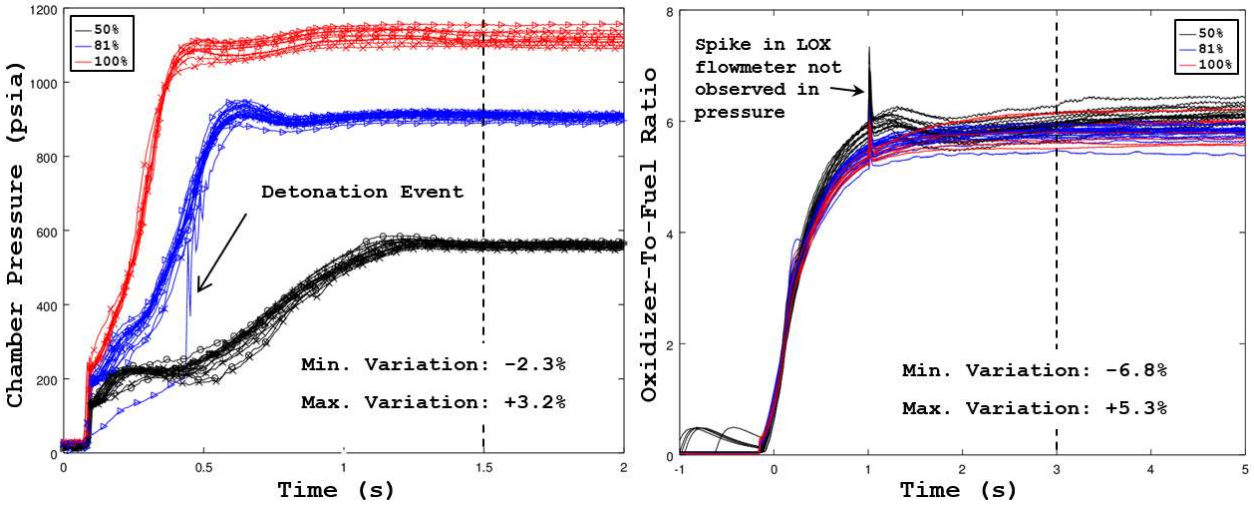

Fig. 7 – Transient Chamber Pressure and O/F Profiles

The most direct indicator of the coupled nozzle/diffuser system start is P_{cell}, which provides a distinctive curve dependent upon the flow field of the nozzle. To illustrate this, the P_{cc} curve of one of the 100% PL tests was taken from data and run in a transient CFD simulation. The results are shown in Fig. 8. When the thruster first begins to fire, P_{cell} remains at approximately 1 atm but begins to fall gently as the free shock separation point within the nozzle pushes to higher area ratios. Free shock separation describes the state in which an overexpanded nozzle incurs boundary layer separation characterized by a lack of reattachment to the nozzle wall. Upon transition to restricted shock separation (in which the boundary layer does reattach to the nozzle), P_{cell} begins to drop sharply. Further information on the FSS and RSS flow structures can be found in [16]. Once the nozzle flows full and the diffuser starts, P_{cell} becomes directly proportional to P_{cc}.

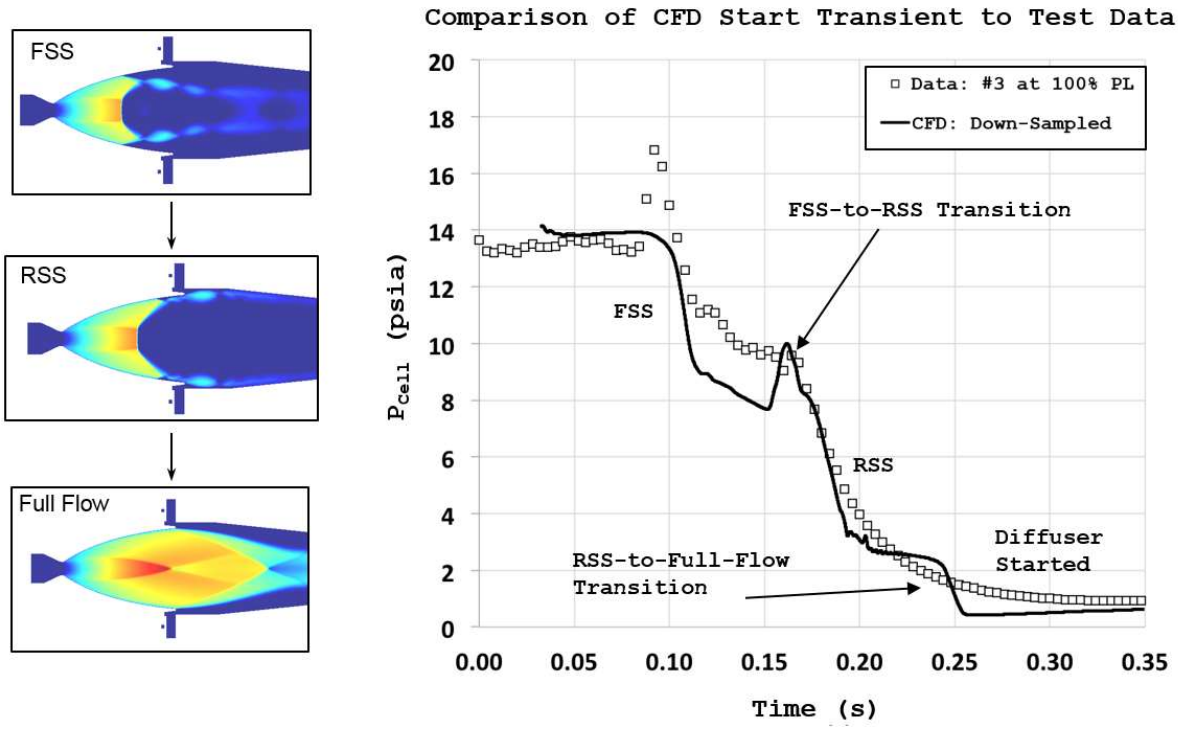

Fig. 8 – Demonstration of Nozzle Flow Structure Effect on P_{cell}

Fig. 9 shows the start and shutdown curves for all power levels and diffusers in a normalized framework. The gap between the two curves is a clear indication of the standard hysteresis effect commonly observed in second throat diffusers. The start and shutdown curves of diffuser #4 at 50% thruster PL are also shown with and without the exit spray ring's influence. A direct, dimensional comparison between the start curves of the four diffusers is found in Fig. 10. The 50% PL curves were chosen because the start process was stretched compared to the higher power levels and effectively provided a better temporal resolution in the data (evident in Fig. 9). All curves share the same general characteristics, with P_{cell} falling at the same rate and each of the diffusers starting at approximately 40% PL. The only notable difference is that diffuser #1 did not show an elevated P_{cell} between ~15%-25% PL. This phenomenon is attributed to its larger second throat compared to the other diffusers. Smaller second throat area can cause mass to temporarily accumulate in the diffuser inlet and contraction before the increased pressure forces it out.

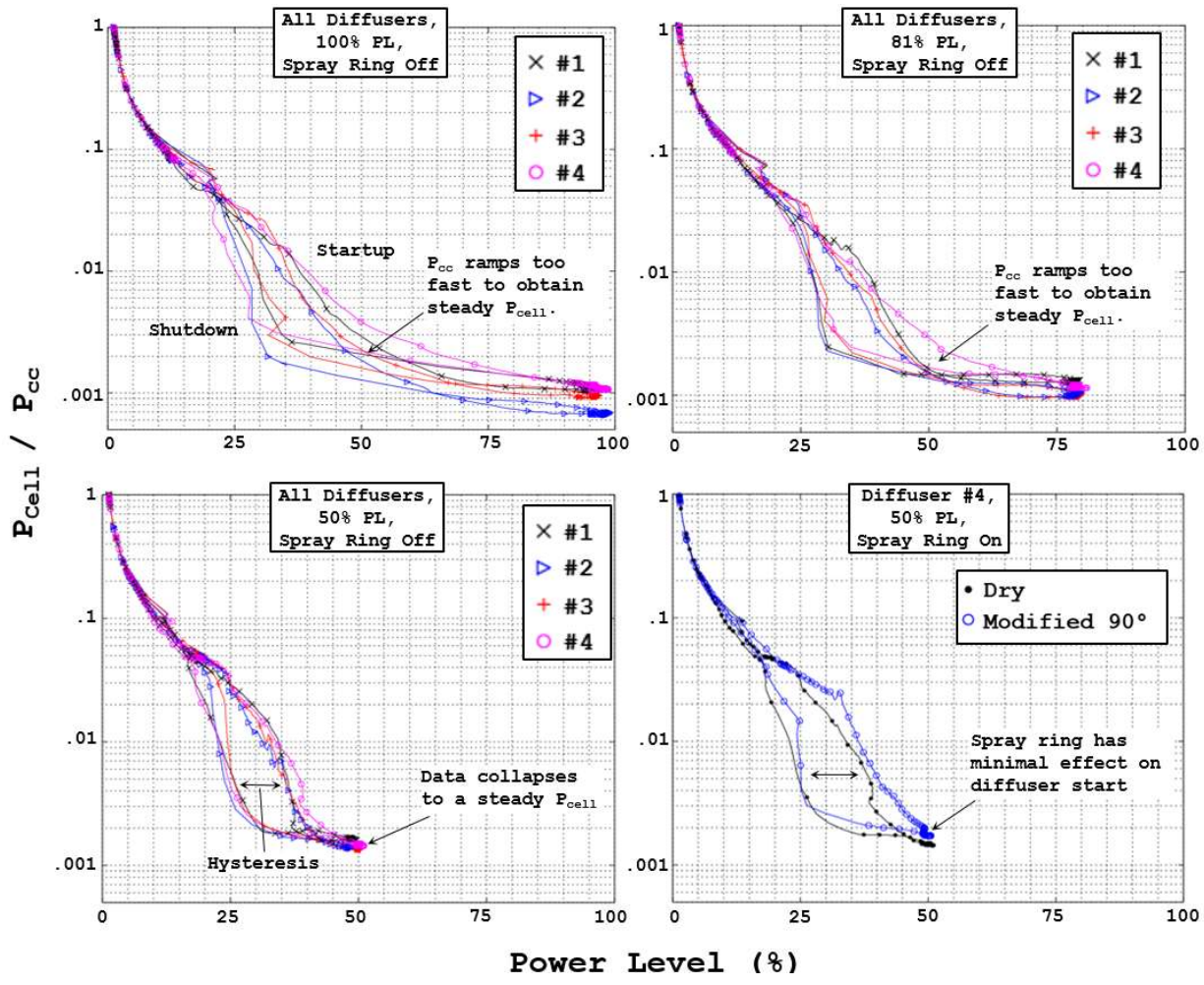

Fig. 9 – Diffuser Start and Shutdown Curves (Normalized)

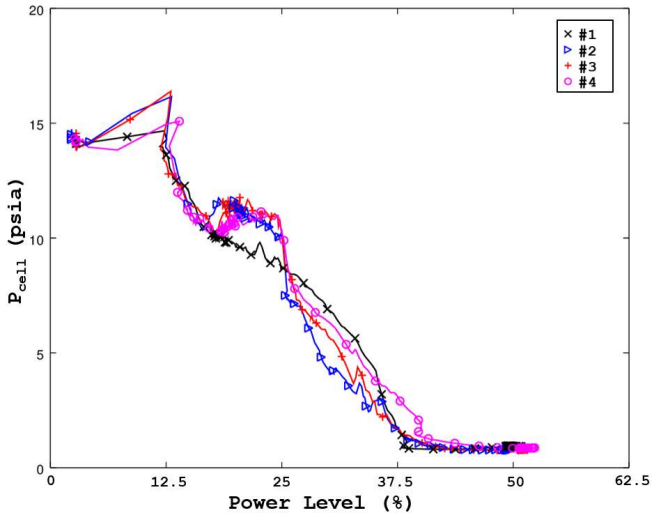

Fig. 10 – Diffuser Start Curves (Absolute)

Steady State Performance

The data in this section was taken from t=1.5s to t=5s, when the thruster's P_{cc} had leveled out and the diffuser flow fields had fully developed to reach an approximately-stable operating condition with respect to P_{cell} and the point of boundary layer separation. Fig. 11 shows the thruster firing through each of the diffusers at the three power levels. The plume becomes less turbulent and more highly-structured with higher power levels and tighter throats, as the point of boundary layer separation is pushed to the end of the diffuser and the entire cross-section of the flow remains supersonic through the exit plane.

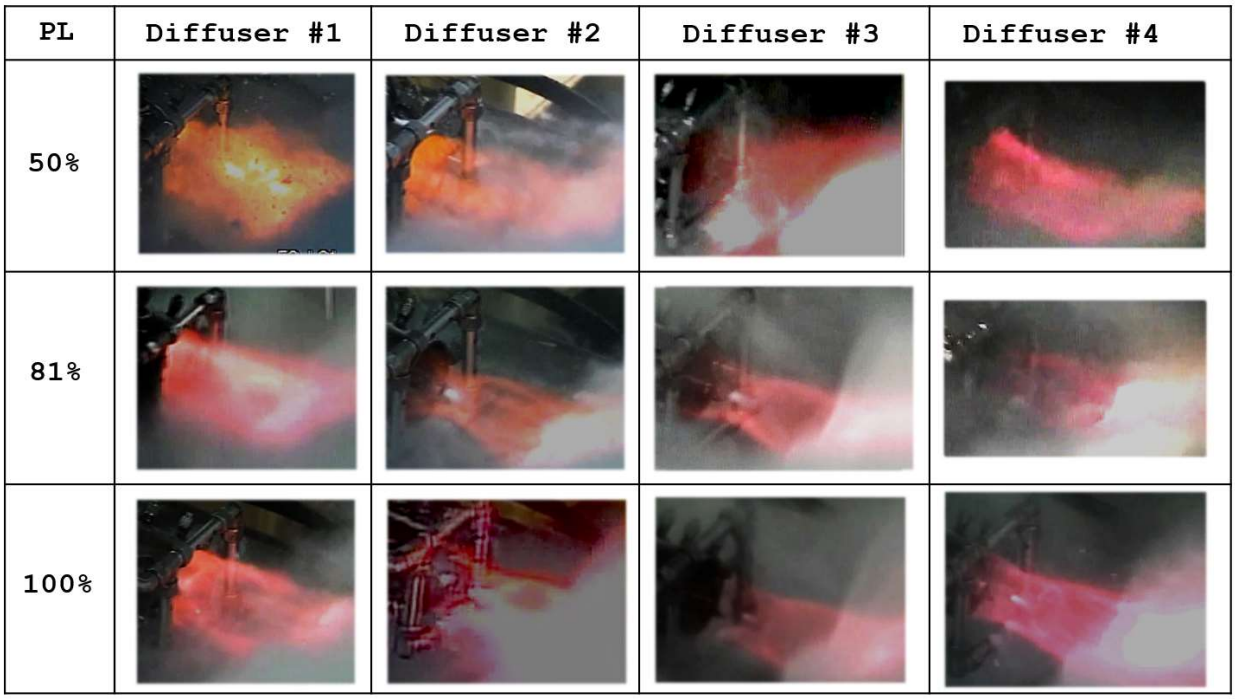

Fig. 11 – Plumes Exiting Diffusers

The location of boundary layer separation within the diffuser serves as a good indicator of aerodynamic performance; less separation typically means the diffuser can pump against a higher back pressure without unstarting. Wall pressure data was captured along each of the diffusers to determine the point of separation for each test. To help interpret the data and evaluate SSC's predictive capabilities, CFD simulations were also performed. Results are given in Fig. 12. At the top of each data set is a visualization of the shock structures

predicted by the CFD. The shock waves are visualized by thresholding the product of the normalized pressure gradient and Mach number. This is very similar to the more common approach of visualizing shocks by thresholding the normal Mach number, but was found to provide a slightly cleaner depiction. Several trends in wall pressure are indicative of particular flow phenomena. Beginning at the diffuser inlet, the wall pressure is very low and approximately P_{cell}. The pressure jumps significantly through the impingement shock then remains relatively low until either boundary layer separation or impingement shock reflection occurs. Boundary layer separation causes a sharp jump in wall pressure followed by a linear rise to ambient conditions at the diffuser exit. Impingement shock reflection also causes a sharp rise in pressure. However, it can be easily distinguished from separation because the downstream pressure decreases as the flow supersonically reaccelerates. When the boundary layer remains attached throughout the diffuser, the shock structure becomes stationary and independent of increasing P_{cc}. As such, the axial variation in wall pressure becomes self-similar, with the magnitude being directly proportional to P_{cc}.

Diffuser #1's 100% PL test data clearly shows all of the behaviors described above. The diffuser inlet maintains ~1.5 psia until impingement, where it jumps to ~7 psia. After impingement, the pressure falls down to the 2-3 psia range until the impingement shock reflection drives it back up to ~7 psia. The plume begins to supersonically reaccelerate and the pressure drops to ~5 psia approximately 3/4 of the way through the throat. However, the boundary layer separates toward the end of the diffuser and the pressure immediately jumps to ~13 psia before rising linearly to atmospheric conditions. CFD simulations were able to predict wall pressures and shock structure with relative accuracy where the boundary layer separation was close (the notable exception being Diffuser #1 at 81% PL).

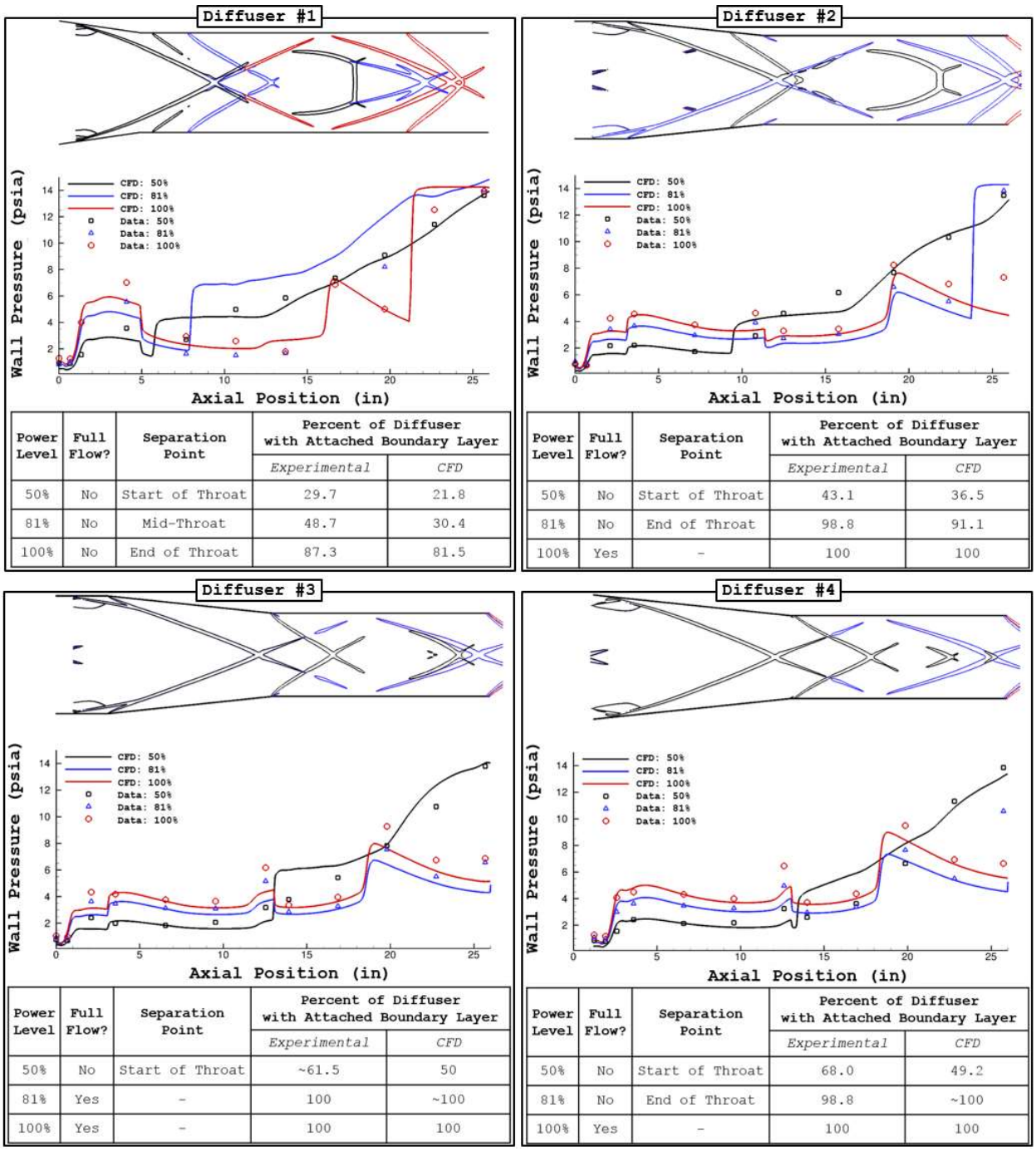

Power Level	Full Flow?	Separation Point	Percent of Diffuser with Attached Boundary Layer	
			Experimental	*CFD*
50%	No	Start of Throat	29.7	21.8
81%	No	Mid-Throat	48.7	30.4
100%	No	End of Throat	87.3	81.5

Power Level	Full Flow?	Separation Point	Percent of Diffuser with Attached Boundary Layer	
			Experimental	*CFD*
50%	No	Start of Throat	43.1	36.5
81%	No	End of Throat	98.8	91.1
100%	Yes	-	100	100

Power Level	Full Flow?	Separation Point	Percent of Diffuser with Attached Boundary Layer	
			Experimental	*CFD*
50%	No	Start of Throat	~61.5	50
81%	Yes	-	100	~100
100%	Yes	-	100	100

Power Level	Full Flow?	Separation Point	Percent of Diffuser with Attached Boundary Layer	
			Experimental	*CFD*
50%	No	Start of Throat	68.0	49.2
81%	No	End of Throat	98.8	~100
100%	Yes	-	100	100

Fig. 12 – Wall Pressure Data and CFD Predictions

A point-by-point comparison of the error in diffuser wall pressure predictions was performed. Fig. 13 shows a graph of the predicted versus measured absolute pressures for all diffusers and engine operating conditions. Ideally, the data should fall along the

1:1 curve. Curves representing +/-20% in prediction error are shown for reference. Overall, the CFD was able to capture the majority of wall pressure measurements within reasonable accuracy. However significant error existed in the predictions for certain cases. To better visualize the trends in these discrepancies, the relative error has been plotted in a histogram format in Fig. 14. The results show that the error generally followed a normal distribution with a standard deviation of 20%. However, this distribution is violated at the positive outer tails of the curve. These errors are a result of the CFD predicting boundary layer separation (i.e. high subsonic pressure) when in fact the diffuser separation was further downstream or non-existent, i.e. low supersonic pressure.

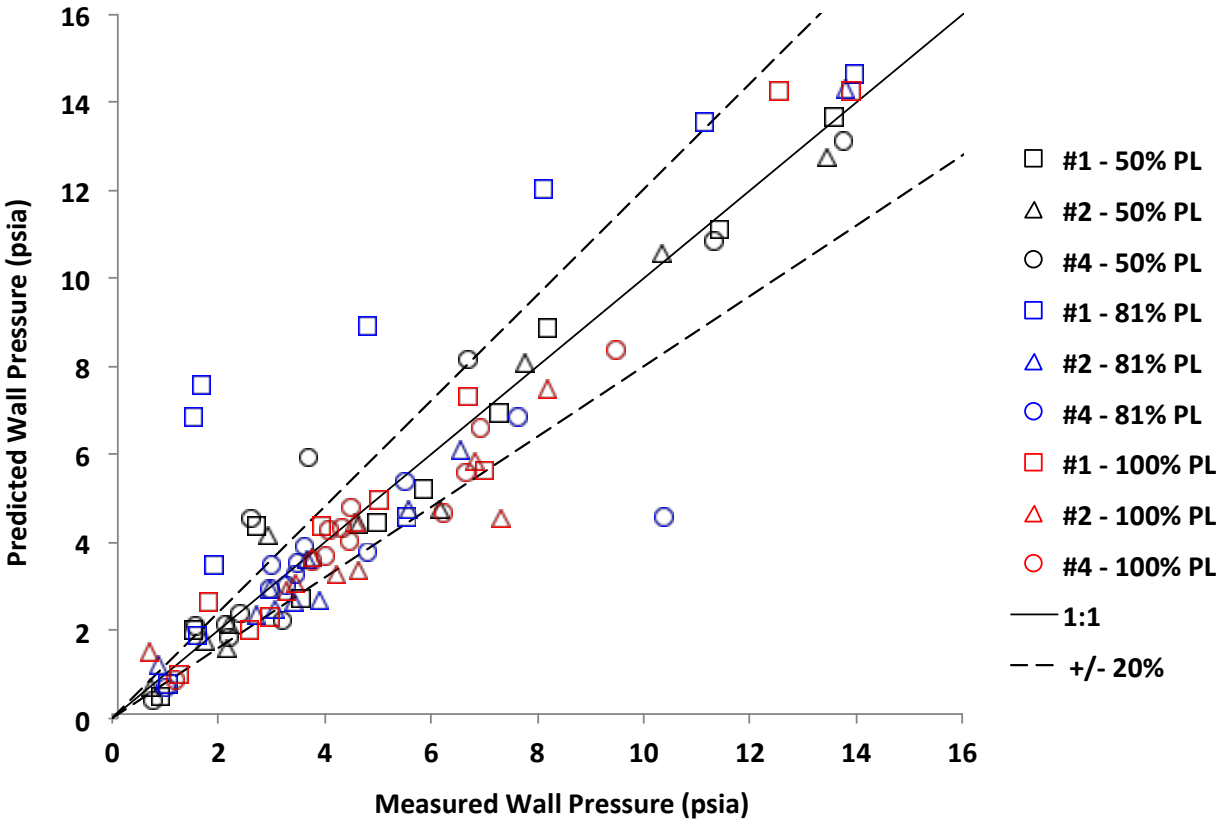

Fig. 13 – Comparison of Predicted to Measured Diffuser Wall Pressures

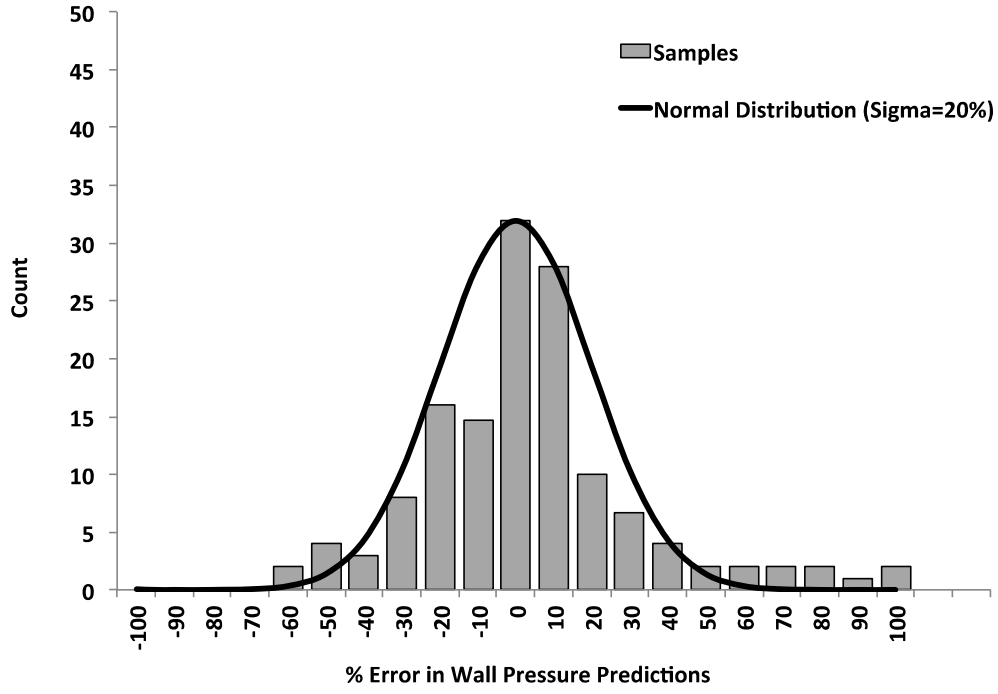

Fig. 14 – Histogram of the Relative Error in Diffuser Wall Pressures

One major conclusion can be reached after further examination of the data presented in Fig. 12: having a tighter second throat greatly benefits performance. Diffuser #1 represents a conservative diffuser design with a relatively large throat based on historical empirical data. It suffers a great deal of boundary layer separation and never flows full. Diffuser #3, however, suffers only half the separation of Diffuser #1 at 50% power level and achieves full flow at 81% PL despite the two having the exact same length. It is important to note, though, that performance gains from tighter throats only occur down to a certain minimum throat area, after which pressure builds within the diffuser contraction and prevents the plume's expansion to the diffuser inlet. The minimum throat area has been determined in a variety of ways through the years [1,2]. Fig. 15 shows a comparison of the diffusers tested in this series of experiments to several methods of determining minimum diffuser throat sizes. All diffusers started without trouble, despite three of them having throat areas below at least one of the historical minima. A possible explanation of this discrepancy is discussed in NASA Technical Memorandum 2016-219219 [3].

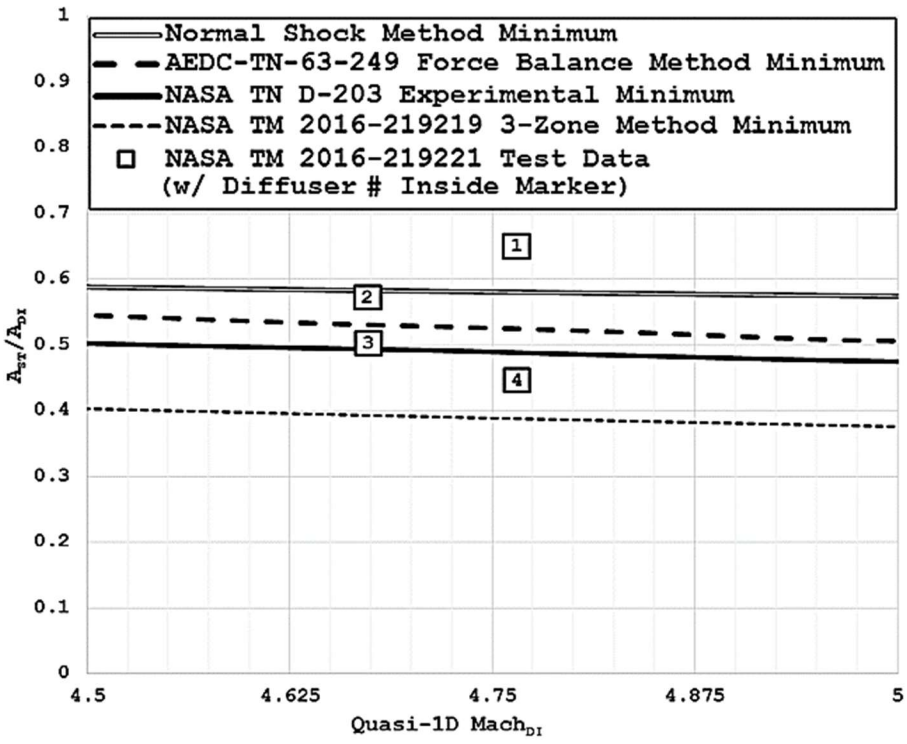

Fig. 15 – Diffuser Contraction Ratios Compared to Various Minima

Water Spray Ring Sensitivity

To assess the impact of water spray at the exit of the diffusers, tests were run both with the spray ring turned off (but with the deflector plate water still on), and with the spray injected 0°, 45°, and 90° to the axis of the plume at a fixed mass flow rate of 26.4 lbm/s (190 gpm). Fig. 16 shows mean pressure and pressure fluctuation as a function of axial position in each of the diffusers. Pressure fluctuation is defined in the figure as the root-mean-square value of pressure normalized by the mean of the measured local pressure. At 50% power level, diffusers #1-3 were relatively unaffected by the axial and 45° injection cases but suffered increased back pressure when subjected to a 90° water flow. This was determined to be a result of water splashback and entrainment into the diffuser. As such, the "Modified 90°" condition was contrived as a way to create positive axial flow and prevent such an effect while still retaining strong plume penetration. In practice, this indicated that the water was injected at an unmeasured angle slightly less than 90°. Also noteworthy at the 50% power level are the strong pressure oscillations

in diffusers #3 and #4, resulting from unsteady boundary layer separation around the transition from contraction to throat. The addition of water spray suppressed this oscillation in all cases, likely by increasing the effective back pressure on the diffusers and pushing the separation away from that unsteady transition point. It is suspected that diffusers #1 and #2 would also experience such oscillatory behavior at some power level between 50% and 81%, when their respective separation points hover around the throat transition. At the 81% and 100% power levels, all diffusers showed substantially decreased sensitivity to water spray injection angle. The higher power level data from diffuser #4 is displayed as an example of this, and shows that the spray ring has no significant effect on internal pressure distribution or fluctuations.

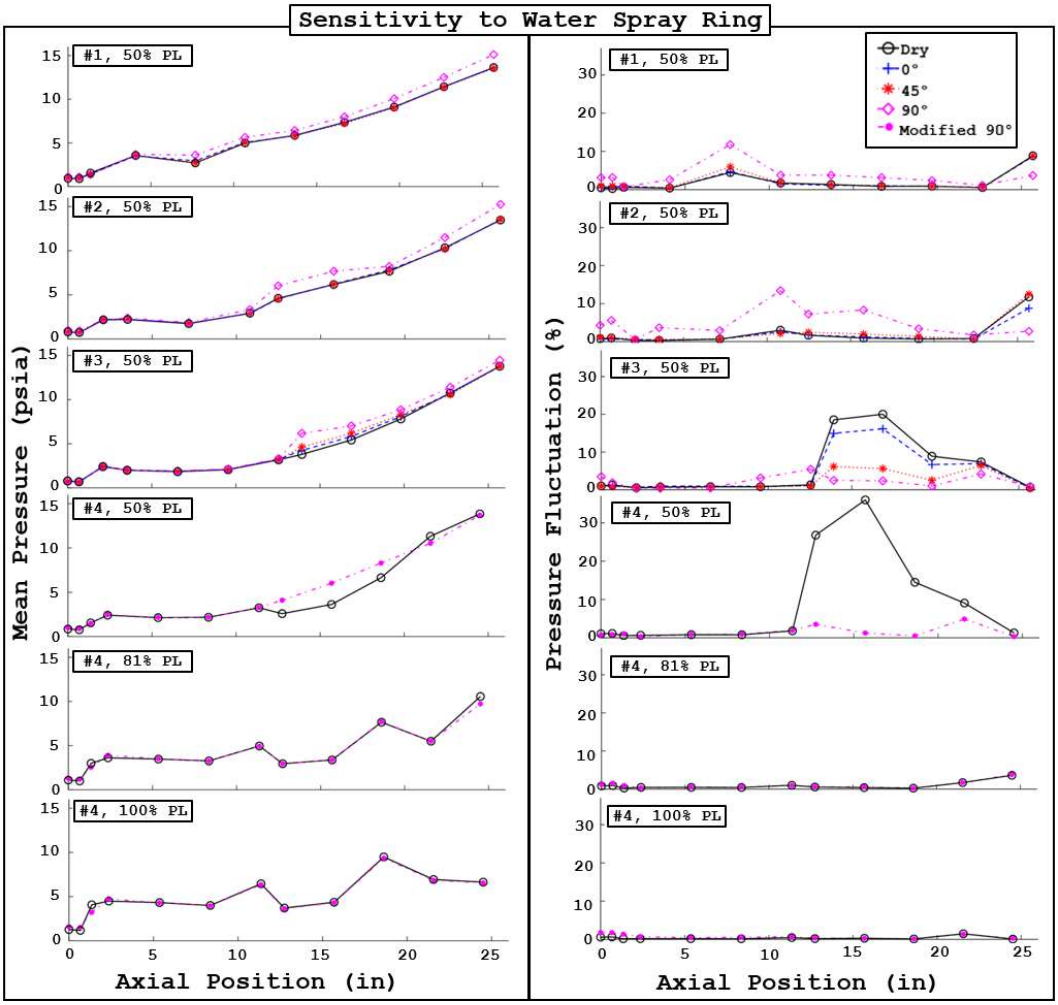

Fig. 16 – Effects of Spray Ring on Wall Pressure

Secondary Flow: GN_2 Purge

GN_2 purge supply pressure was varied from 100-2000 psia to show the sensitivity of test cell pressure to the purge flow rate. The results are shown in Fig. 17, accompanied by data from J-2X testing at SSC's A-2 test stand for comparison. Diffuser #2 shows only relatively small increases in P_{cell} with large increases in purge flow rate, while the A-2 diffuser and diffuser #1 are much more sensitive. This is because Diffuser #2 has a cylindrical inlet and therefore a fixed impingement area ratio. The other two diffusers have conical inlets, so as the purge mass flow is increased, the higher velocity flow into the diffuser inlet pushes the plume's impingement forward to lower area ratios. This has the effect of reducing the plume's expansion and increasing P_{cell} much more substantially at higher purge rates.

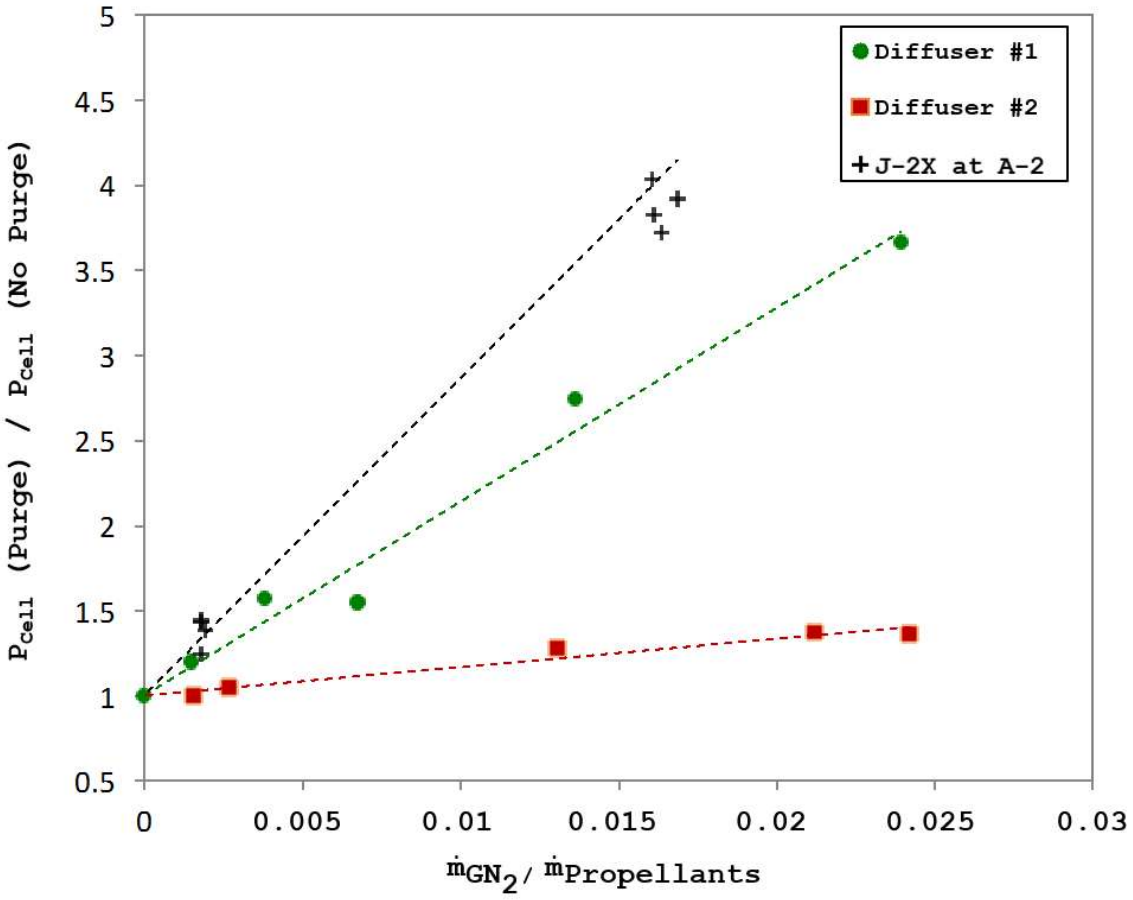

Fig. 17 – Effects of GN_2 Purge Flow Rate on Test Cell Pressure

THERMAL ENVIRONMENTS

One of the major challenges in the deployment of passive diffusers is dealing with the heat transfer generated by capturing the rocket plume and forcing it to contract. Doing so concentrates the energy and ensures contact between the hot plume and the diffuser wall. To assess the differences in heat flux between geometries, fast-response thermocouples were installed along the diffusers in the same axial locations as the pressure transducers. The assumption of 1-D heat conduction in a semi-infinite slab was made to enable the calculation of heat transfer from temperature data using the Cook-Felderman Technique as described in [17]. The computed heat fluxes are given as a function of axial position in Fig. 18 and are plotted alongside CFD cold-wall predictions for comparison. Incomplete data sets are the result of sensor malfunctions during testing. Similar to wall pressure, heat transfer displays characteristic behaviors indicative of particular flow phenomena. The diffuser walls receive relatively little heat upstream of plume impingement. However, the initial contact point endures a very high heat load (> 125 BTU/ft^2/s). As the plume passes through the contraction and into the throat, the heating rate drops up to 50%. Additional localized peaks can be caused by the Mach disks (as with diffuser #1 at 50% PL), boundary layer separation, and impingement shock reflection within the throat. Regions unaffected by boundary layer separation have heat fluxes that are effectively proportional to P_{cc} since the flow structure remains fixed. This is easily visible in the diffuser #4 data. Heat flux also generally increased with smaller throat area.

Taken point-by-point, CFD was not consistent in predicting the magnitude of heat transfer. However, the simulations still proved very useful in predicting trends and interpreting the data. Table 7 provides the heat flux data averaged over the entire length of the diffusers. Although the CFD-predicted magnitude of heat transfer at any given point along the diffuser might have been off, the average over the entire length was relatively close to data, with a maximum error of less than 20% and average error of 7%.

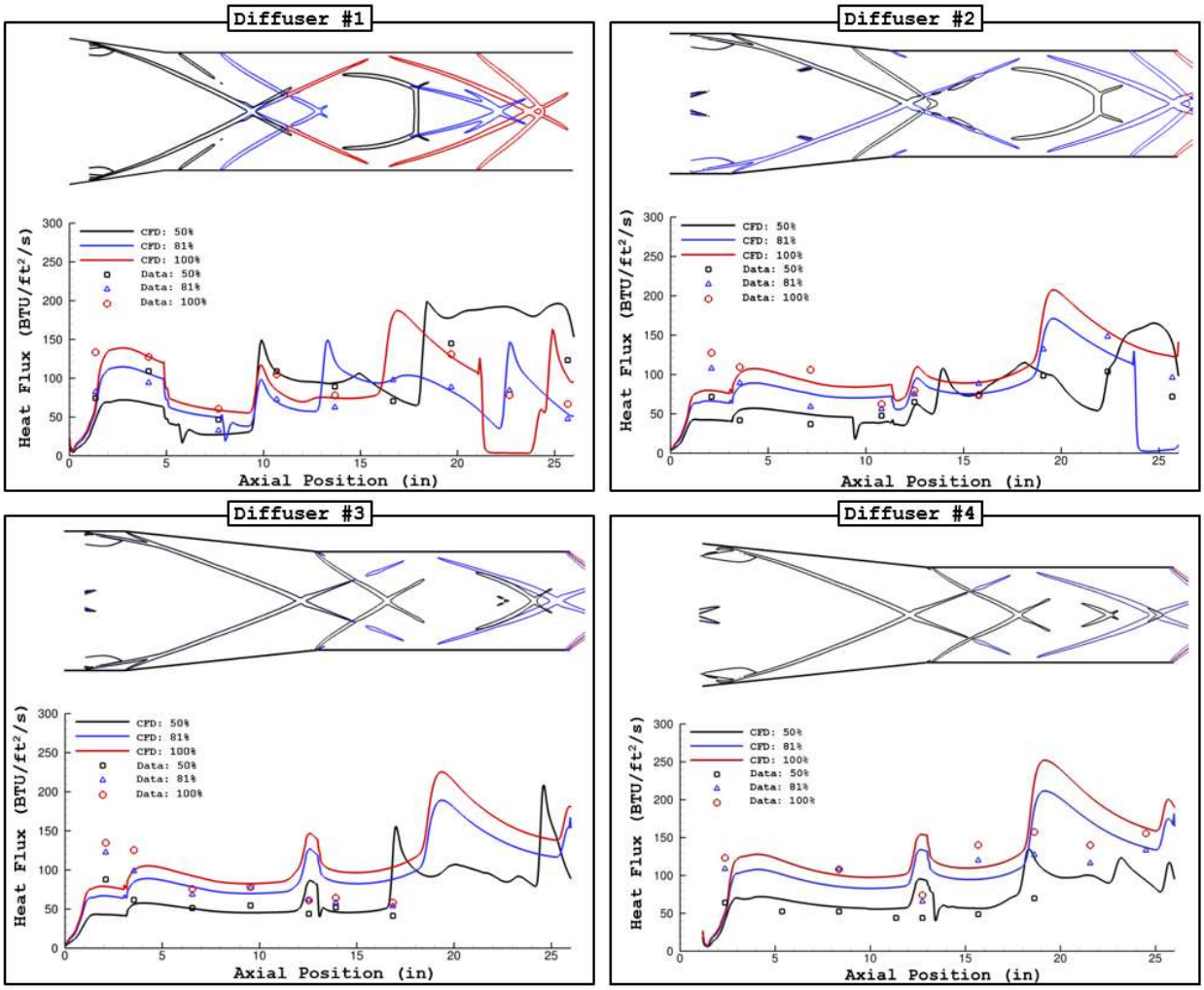

Fig. 18 - Data and CFD Predictions of Local Heat Flux

	50% PL			81% PL			100% PL		
Diffuser	**Data**	**CFD**	**Percent Error**	**Data**	**CFD**	**Percent Error**	**Data**	**CFD**	**Percent Error**
#1	95.9	94.9	-1.0	76.9	76.2	-0.9	97.6	85.7	-12.2
#2	67.9	65.5	-3.5	94.7	76.4	-19.3	99.2	99.8	+0.60
#4	-	-	-	101.9	109.3	+7.3	146.0	129.1	-11.6

Table 7 - Average Diffuser Heat Fluxes (BTU/ft²/s)

CONCLUSIONS

In this report, the results of hot-fire rocket testing with four passive second-throat diffusers have been presented and compared to CFD predictions of wall pressure and heat transfer. Sensitivities of diffuser performance to nitrogen purge and exit spray water were quantified and found to be small, though some water injection configurations excited strong acoustic modes. Sensitivity of boundary layer separation to second throat size was also evaluated, with performance augmentation noted at lower throat areas. CFD was shown to qualitatively reproduce internal flow structures and predict limiting diffuser throat size more accurately than historical techniques for this test configuration. One of the biggest challenges in modeling the current rocket diffusers was to consistently predict boundary layer separation. In cases where boundary layer separation was captured correctly, accuracy in the predicted wall pressures was acceptable. However, substantial error was observed in some cases where the CFD over-predicted the sensitivity of the boundary layer resulting in excessive flow separation.

REFERENCES

[1] Jones, W., Price, H., and Lorenzo, C., "Experimental Study of Zero-Flow Ejectors Using Gaseous Nitrogen," NASA TN D-203, March 1960.

[2] Panesci, J., and German, R., "An Analysis of Second-Throat Diffuser Performance for Zero-Secondary-Flow Ejector Systems," AEDC-TDR-63-249, December 1963.

[3] Jones, D., "Passive Rocket Diffuser Theory: A Re-Examination of Minimum Second Throat Size," NASA TM 2016-219219, April 2016.

[4] Melcher, J., Morehead, R., "Combustion Stability Characteristics of the Project Morpheus Liquid Oxygen / Liquid Methane Main Engine", AIAA Paper 2014-3681, 50th AIAA/ASME/SAE/ASEE Joint Propulsion Conference, Cleveland, OH, July 28-30, 2014.

[5] Saunders, G. P., Raines, N. G., Varner, D. G., "Design, Activation, and Operation of the J2-X Subscale Simulator (JSS)", AIAA Paper 2009-5098, 45th AIAA/ASME/SAE/ASEE Joint Propulsion Conference, Denver, CO, August 2-5, 2009.

[6] Allgood, D., Graham, J., Ahuja, V., and Hosangadi, A., "Computational Analyses in Support of the Sub-scale Diffuser

Testing for the A-3 Facility - Part 1: Steady Predictions," AIAA Paper 2009-5098, 45th AIAA/ASME/SAE/ASEE Joint Propulsion Conference, Denver, CO, August 2-5, 2009.

[7] Allgood, D., Lott, J., and Raines, N., "Ablative Rocket Deflector Testing and Computational Modeling," 57th JANNAF Propulsion Meeting, Colorado Springs, CO, May 3-7, 2010.

[8] Sachdev, J. S., Ahuja, V., Hosangadi, A., and Allgood, D., "Analysis of Flame Deflector Spray Nozzles in Rocket Engine Test Stands," AIAA Paper 2010-6972, 46th AIAA/ASME/SAE/ASEE Joint Propulsion Conference, Nashville, TN, July 25-28, 2010.

[9] Allgood, D., Saunders, G. P., and Langford, L., "Reduction of Altitude Diffuser Jet Noise Using Water Injection," AIAA Paper 2012-0680, 50th AIAA Aerospace Sciences Meeting, Nashville, TN, January 9-12, 2012.

[10] Rao, G.V.R., "Exhaust Nozzle Contour for Optimum Thrust", Journal of Jet Propulsion, Vol. 28, No. 6, p. 377-382, June 1958.

[11] Rao, G.V.R., "Approximation of Optimum Thrust Nozzle Contour," ARS Journal, Vol. 30, No. 6, p. 561, June 1960.

[12] Luke, E., and George, T., "Loci: A Rule-Based Framework for Parallel Multidisciplinary Simulation Synthesis," Journal of Functional Programming, Volume 15, Issue 03, 2005, pp. 477-502, Cambridge University Press.

[13] Luke, E., Tong, X., Wu, J., Cinnella, P., and Chamberlain, R., "CHEM 3.3: A Finite-Rate Viscous Chemistry Solver - The User Guide," January 2013.

[14] Shang, H.M., Chen, Y.S., Liaw, P., Chen, C.P. and Wang, T.S., "Investigation of Chemical Kinetics Integration Algorithms for Reacting Flows," AIAA Paper 95-0806, 33rd Aerospace Sciences Meeting and Exhibit, Reno, NV, Jan 1995.

[15] Allgood, D.C., "Development of Detonation Modeling Capabilities for Rocket Test Facilities: Hydrogen-Oxygen-Nitrogen Mixtures," NASA/TP-2016-219220, April 2016.

[16] Östlund, J., "Flow Processes in Rocket Engine Nozzles with Focus on Flow Separation and Side-Loads," Technical Report 2002:09, Department of Mechanics, Kungl Techniska Högskolan, Stockholm, Sweden, 2002.

[17] Battisti, L., and Bertolazzi, E., "Thin Film Heat Transfer Data Reduction by Means of Some Numerical Techniques", Tech. Rep. #15, Dept. of Mechanical and Structures Engineering, Trento University, Italy, 2001.